Superpressure Balloon Observations of
Pressure and Temperature Fluctuations in the Stratosphere
and their Spectral Characteristics

by

Elizabeth Patrice Quinn

A thesis submitted in partial fulfillment
of the requirements for the degree of

Master of Science

University of Washington

1987

Approved by _____
(Chairperson of Supervisory Committee)

Program Authorized
to Offer Degree _____

Date _____

Master's Thesis

In presenting this thesis in partial fulfillment of the requirements for a Master's degree at the University of Washington, I agree that the Library shall make its copies freely available for inspection. I further agree that extensive copying of this thesis is allowable only for scholarly purposes, consistent with "fair use" as prescribed in the U.S. Copyright Law. Any other reproduction for any purposes or by any means shall not be allowed without my written permission.

Signature_____

Date _____

ABSTRACT

Pressure and temperature data from eight superpressure balloon flights at 26 km in the southern hemisphere stratosphere are analyzed. The balloons travel steadily westward during summer and eastward during winter as expected from local climatology. Two types of fluctuations are observed; neutral bouyancy oscillations (NBO) of around 4 minutes, and 0.1 to 1 hour oscillations which are characterized as small amplitude fluctuations. Lapse rates and densities are calculated and found to agree well with the expected values. Interesting examples of a large scale disturbance, wave damping, and simultaneous fluctuation at two nearby balloons are noted and examined. Spectral analysis is performed clearly showing the NBO, and some peaks at lower frequency with more power than the NBO. The majority of the power is in the long period range. Spectral slopes are measured to be on the average -2.30 ± 0.24 for pressure, and -1.76 ± 0.26 for temperature. These slopes are consistent with observations elsewhere, but they do not clearly differentiate between turbulence theory and the universal gravity wave spectrum theory.

TABLE OF CONTENTS

LIST OF FIGURES

LIST OF TABLES

ACKNOWLEDGEMENTS

The author wishes to thank Professor Bob Holzworth for his help, patience, and support throughout this project. In addition, thanks to Professor Conway Leovy for his time and insights. Thanks also to Professor Miguel Larsen and Dr. Justin Smalley for their helpful comments.

INTRODUCTION

Gravity waves play an important role in the study of atmospheric dynamics. Investigators have found that waves, in the course of their generation, propagation, and dissipation, extract, transport, and deposit amounts of energy and momentum large enough to be significant to the global atmospheric energy and momentum balance (Gossard, 1975).

The earliest work on gravity waves was stimulated by the wave like structure of billow clouds. Some argued that billow clouds were a manifestation of interface waves. In 1929 Johnson published an analysis of pressure fluctuations in Britain, which he attributed to waves traveling on density interfaces within the atmosphere (ef. Gossard, 1975).

Hines (1960) proposed a theory describing the observed atmospheric fluctuations as manifestations of the (upward) propagation of internal gravity waves. Hines (1960) also anticipated some of the important effects of gravity waves in the middle atmosphere, including the transport of energy, the generation of turbulence, the likelihood of a nonlinear cascade of energy to smaller-scale waves as a result of large gravity wave amplitudes, and the possible modulation of the middle atmosphere response due to the variable characteristics and energies of gravity waves propagating up from below.

Houghton (1978) suggested that gravity waves are the most likely candidate for balancing the thermal and momentum budgets of the middle atmosphere because of their known sources in the lower atmosphere, their ability to transport momentum vertically, and their convergence of momentum flux in regions of (turbulent) dissipation. The principal sources of gravity waves in the lower atmosphere are thought to be topography, wind shear, and convection, though many others, such as geostrophic adjustment and frontal accelerations contribute as well (Fritts, 1984).

Momentum deposition accompanying gravity wave dissipation was suggested by Houghton (1978) and Lindzen (1981) to provide the momentum source needed to satisfy the thermal and momentum budgets of the middle atmosphere. Holton (1982) succeeded in reproducing the gross features of the summer solstice circulation and an annual cycle with his crude gravity wave source spectrum. In the mesosphere and lower thermosphere, gravity wave drag results in a reversal of the vertical shear of the zonal mean wind, driving a strong mean meridional circulation and a reversal of the mean meridional temperature gradient near the mesopause (Fritts & Rastogi, 1985). The effects of gravity wave drag in the stratosphere, while not as significant as at higher levels, appear to be important in maintaining the large scale circulation of this region (Fritts & Rastogi, 1985).

In the troposphere, spectacular records of waves have been observed with a frequency-modulated continuous wave radar sounder developed by Richter (1969). Many recent investigations have used radar sounding to observe waves. Larsen et al (1982), Larsen and Swartz (1982), and Lu et al (1985) have all made radar measurements of gravity waves in the atmosphere. However due to radar sensitivity limitations, the maximum altitude the soundings reached in these studies was 24 km.

Another method for measuring gravity waves is the superpressure or constant volume balloon. Cadet (1978) states "One peculiar quality of a superpressure balloon is it's relative stability on a constant density surface." This stability is quite important when studying phenomena having a weak amplitude, such as gravity waves. Many important features of gravity waves are not well understood, and need further investigation such as their propagation in the lower stratosphere, their relationship with atmospheric instability, and their relationship to three-dimensional turbulence.

In this work we will look at constant volume balloon data from the EMA (Electrodynamics of the Middle Atmosphere) study. EMA is an experiment in which eight small superpressure balloons were launched from Christchurch, New Zealand during 1983 through early 1984 (Holzworth, 1983). The altitude at which these balloons floated was approximately 26 km.

This is the first study of it's kind at 26 km. The primary payload instrument measures the vector electric field from DC to 10 kHz. Other detectors included instruments to measure localized ionization rate, electrical conductivity, magnetic field, pressure and temperature fluctuations, and to record optical lightning (Holzworth, 1983). Figures 1 a and b are pictures of an EMA payload and balloon. The pressure sensor is inside the styrofoam box, and the redundant temperature sensors are mounted on 18 inch wire booms from two opposite corners of the bottom of the payload (inside the circle in figure 1a).

In this work we will be looking at the temperature and pressure fluctuations. We will identify the neutral bouyancy oscillation (NBO) of the balloons which is about 3.5 to 4.5 minutes, and then look at waves with periods greater than the NBO. We will calculate the temporal power spectra for pressure and temperature, and discuss our results in the context of turbulence, and a universal gravity wave spectrum.

The conclusions we will draw include that the balloons travel as would be expected from the climatology with no evidence for large scale 2-D turbulence or large scale inertial oscillations. That the calculated lapse rates and densities are as expected for the 26 km level, and that the balloons do travel on a constant density surface. During the time when EMAs 4 and 5 are close together (within 500 km), if they see the same oscillation then the

a.

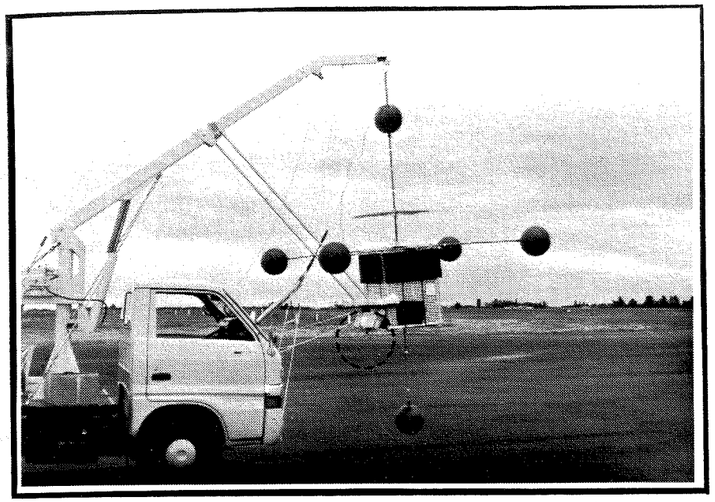

b.

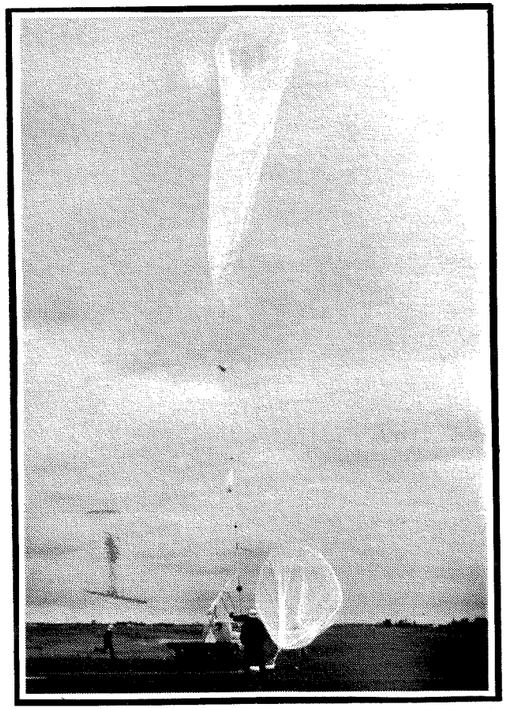

FIGURE 1. (a) EMA payload. (b) EMA balloon being launched.

horizontal wavelength of that oscillation must be on the order of 500 km or more. Spectral analysis clearly shows the NBO, as well as the occurence of significant longer period peaks in some spectra. No obvious correlation was found between cloudiness and enhanced power. Spectral slopes were found to be in good agreement with other recent studies. They are well correlated with the values predicted by turbulence theory, and partially correlated with values predicted by the universal gravity wave spectrum theory.

SUPERPRESSURE BALLOON DESCRIPTION AND HISTORY

Superpressure or constant volume balloons are non-extensible balloons that float on a constant density surface. As a small superpressure balloon rises the gas fills out the balloon. A height is reached at which the balloon is completely inflated and begins to overpressure. When the mass of the balloon system and the mass of the displaced air become equal, the bouyant and gravitational forces balance, and the balloon reaches hydrostatic equilibrium (Lally,1975). As long as the balloon remains superpressured it will continue to float at a constant density level. If the superpressure balloon is displaced from it's bouyancy altitude there is a restoring force proportional to the balloon volume and density difference (Lally, 1975).

The U.S. became interested in the study of constant level balloons after the Japanese used unmanned balloon bombs at the end of WWII. In 1948 the U.S. developed a horizontal balloon system for the study of air trajectories, and in 1950 the U.S. Navy proposed the use of balloons for collecting meteorological data over the oceans. Between 1957 and 1959, 100 balloons floated across the Pacific at a height of 9000 m. They were tracked by a radio direction finder (Cadet, 1978).

In 1960, Lally proposed the use of satellites in polar orbit to determine balloon positions. During the sixties technical advances in the manufacture of strong plastic films and microminiature electronics made constant level balloons, as we know them today, possible. Through the sixties constant level balloons remained a valuable tool for meteorological research (Cadet, 1978).

One of the first large scale constant level balloon experiments was the GHOST (Global HOrizontal Sounding Technique) experiment. During 1966 and 1967 superpressure balloons were launched from New Zealand. The balloons floated at the 200 mb level, and were a source for southern hemisphere flow information (Wooldridge & Reiter, 1970).

In the winter of 1966/67 constant volume balloon, as well as aircraft flights were made to obtain records of tropospheric and stratospheric kinematics and dynamics during typical and extreme conditions of westerly flow across the Continental Divide (Vergeiner & Lilly, 1970). Forty-four balloons were launched yet only 19 successfully reached float altitude. The major cause of failure appeared to be the accumulation of ice/snow on the balloons.

In the early seventies, the Eole experiment took place. Four-hundred and eighty constant level balloons were released from the southern hemisphere. The Eole navigation and data collection satellite tracked the locations of the balloons providing a completely homogeneous set of very accurate in situ measurements of the horizontal wind at the 200 mb level on a planetary scale (Morel and Bandeen, 1973).

In the early to mid seventies, TWERLE (Tropical Wind, Energy Conservation & Reference Level Experiment), a large scale constant-level balloon experiment took place. Levanon et al (1974) analyzed some of the initial

data. They looked at the radio altimeter and pressure sensor data and found four types of altitude changes. The first is the NBO (neutral bouyancy oscillation) which is essentially simple harmonic motion about the equilibrium surface. The second type of oscillations they saw were short term oscillations with a period of $\approx$ 1.2 hrs. The third was a diurnal half cycle, and the forth were possible trends of up to $\approx$120m/day possibly caused by drift of the sensors (Levanon et al, 1974).

TWERLE data was collected using the Nimbus-6 satellite doppler location system (The TWERLE Team, 1977). Three hundred and ninety-three TWERLE balloons were successfully launched. The balloon platforms floated at the 150mb level. The basic data is quasi-Lagrangian (travels with the flow on a constant density surface) in nature. The motions investigated and discussed by the TWERLE Team (1977) are gravity waves, orographic lee waves, and forced flow over developing convection clouds.

Variance spectra of observed air density were calculated, and peaks were seen at 4.3 min, 6-7.5 min, 24 min, and 38 min. The 4.3 min peak was the NBO. The 6-7.5 min peaks were attributed to lee waves, and the 24 and 38 min peaks were attributed to gravity waves. Another interesting feature of the TWERLE data was the large number of waves clustered around the tip of South America. The TWERLE experiment demonstrated the extraordinary flexibility and utility of an instrumented superpressure balloon system using satellite data collection and location determination.

The superpressure balloon is potentially well suited for the study of gravity waves because the data is quasi-Lagrangian in nature and because superpressure balloons have the advantage of providing high resolution data of small scale structures.

NBO

Neutral bouyancy oscillations (NBO) or oscillations about the equilibrium density surface have been described by many people (Lally, 1975; Levanon et al, 1974; Massman, 1978a). From the equation of motion of the balloon it is possible to derive the period of the neutral bouyancy oscillation.

The balloon equation of motion (Massman, 1978a) is

$$M_b \frac{d\vec{v}}{dt} = -\tfrac{1}{2} M_a \frac{d(\vec{v}-\vec{u})}{dt} - \tfrac{1}{2} \rho_a C_d A_b (\vec{v}-\vec{u}) \mid \vec{v}-\vec{u} \mid + M_a \frac{d\vec{u}}{dt} + (M_b - \rho_a V_b)\vec{g} \qquad (1)$$

where

A_b balloons cross-sectional area

C_d drag coefficient

$\vec{g}$ acceleration due to gravity

M_a mass of air displaced by balloon system

M_b mass of balloon system

ρ_a density of air displaced by balloon

$\vec{u}$ three dimensional velocity of atmosphere

$\vec{v}$ three dimensional velocity of balloon

V_b volume of balloon.

The term on the left hand side is the net force. The first term on the right hand side is the inertial drag. The second is the aerodynamic drag. The third is the atmospheric driving force, and the last term is the bouyancy force.

As shown by Levanon et al (1974), the vertical component of the equation of motion, assuming that the balloon drag acceleration and the atmospheric acceleration are negligible, is given by

$$M_b \frac{d^2 z}{dt^2} = (\rho_a V_b - M_b) g - \frac{1}{2} M_a \frac{d^2 z}{dt^2}. \qquad (2)$$

Near equilibrium $M_a \approx M_b$ and equation (2) reduces to

$$\frac{3}{2} M_b \frac{d^2 z}{dt^2} = (\rho_a V_b - M_b) g. \tag{3}$$

Levanon et al (1974) show that by taking into account the fact that as the balloon oscillates, the density and pressure of the surrounding atmosphere change causing the balloon volume to expand and contract, equation (3) can be rewritten to close approximation as

$$\frac{d^2 z}{dt^2} = \frac{2}{3} g \left(\frac{1}{\rho_0} \frac{\partial \rho_a}{\partial z} (1 + \frac{1}{V_0} (\frac{\partial V}{\partial P})_T \Delta P) \right) (Z - Z_0) \tag{4}$$

where ρ_o is the density at equilibrium, V_o is the volume of the balloon at equilibrium, ΔP is the superpressure at equilibrium, and Z_o is the static equilibrium height.

Using the ideal gas law and hydrostatic equilibrium, and ignoring the slight variations in the balloons volume as suggested by Massman (1978a), equation (4) becomes

$$\frac{d^2 z}{dt^2} = \frac{2}{3} g \left(-\frac{g}{r T_0} - \frac{1}{T_0} \frac{\partial T}{\partial z} \right) (Z - Z_0) \tag{5}$$

where r is the universal gas constant. This is the familiar equation of simple harmonic motion with the period of oscillation, τ, equal to

$$\tau = 2\pi \left(\frac{3}{2} \frac{1}{g} \frac{T_0}{(\frac{g}{r} + \frac{\partial T}{\partial z})} \right)^{\frac{1}{2}}. \tag{6}$$

For our data the equilibrium surface is at $\approx$26km. Taking $T_0 = 222.65^o K$, and $\frac{\partial T}{\partial z} = 1^o$ K/km from appendix E of Holton (1979) one gets that $\tau \approx 195$ sec, or that the NBO period is approximately 3.3 min.

Table 1 shows various values of τ for different values of T_o and $\frac{\partial T}{\partial z}$. Mass-man (1978a) calculated τ for the troposphere to be between 190 and 217 seconds, and calculated τ for the stratosphere to be between 186 and 209 seconds, in good agreement with our calculations.

Figure 2 is a sample of the real time pressure measurement from flight #4. One can clearly see the regular 4 min neutral bouyancy oscillations. The pressure changes $\approx$ 0.1 mb during a NBO which corresponds to a vertical variation of $\approx$ 12 meters.

$T_o\,(^\circ K)$	$\frac{\partial T}{\partial z}(^\circ K/km)$	$\tau(sec)$
213.15	2.0	189
223.15	0.0	199
223.15	1.0	196
223.15	2.0	193
233.15	2.0	197

TABLE 1. Predicted period of the NBO.

GRAVITY WAVES

In general a wave is a perturbation on a steady, slowly changing background (Beer, 1972). Gravity or bouyancy waves can only exist when the atmosphere is stably stratified (lower density over greater density). Then a vertically displaced parcel will undergo bouyancy oscillations. The restoring force is the bouyancy force (Holton, 1979).

The solutions for two-dimensional gravity waves in the atmosphere are very similar to the solutions for oceanic gravity waves. It is assumed that

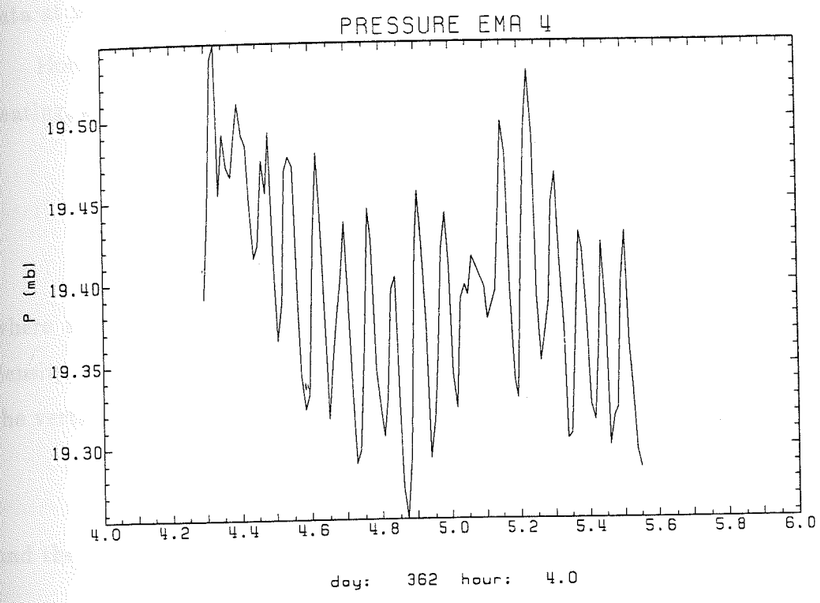

FIGURE 2. Real time pressure data from EMA 4 day 364. One can clearly see the 4 min neutral bouyancy ocsillations.

the atmosphere is incompressible and the Boussinesq approximation (that density = a constant except where coupled with gravity) is employed. Also only vertical motions << the atmospheric scale height (≈6.6 km for our data at 26 km altitude) are considered for 2-D turbulence in the x-z plane.

Holton (1979) shows that in this approximation, and neglecting rotation, heating, and dissipation the equations of motion are

$$\frac{\partial u}{\partial t}+u\frac{\partial u}{\partial x}+w\frac{\partial u}{\partial z}+\frac{1}{\rho}\frac{\partial p}{\partial x}=0, \text{ and} \tag{7}$$

$$\frac{\partial w}{\partial t}+u\frac{\partial w}{\partial x}+w\frac{\partial w}{\partial z}+\frac{1}{\rho}\frac{\partial p}{\partial z}+g=0 \tag{8}$$

where u = horizontal velocity, w = vertical velocity, p = pressure, ρ = density, t = the time coordinate, x = the horizontal coordinate, and z = the vertical coordinate. The continuity equation is

$$\frac{\partial u}{\partial x}+\frac{\partial w}{\partial z}=0, \tag{9}$$

and the equation of state is

$$\frac{\partial \theta}{\partial t}+u\frac{\partial \theta}{\partial x}+w\frac{\partial \theta}{\partial z}=0 \tag{10}$$

where θ = potential temperature. The potential temperature is related to the pressure and density by $\theta=\frac{p}{\rho R}(\frac{p_s}{p})^k$ where R = the gas constant for dry air, p_s = standard pressure usually taken to be 1000 mb, and $k=\frac{R}{C_p}$ where C_p is the specific heat at constant pressure.

Now the equations are linearized by letting $\rho=\rho_o+\rho'$, $p=\overline{p}(z)+p'$, $\theta=\overline{\theta}(z)+\theta'$, $u=u'$, and $w=w'$, and employing the hydrostatic approximation to give the linearized set of equations.

$$\frac{\partial u'}{\partial t}+\frac{1}{\rho_0}\frac{\partial p'}{\partial x}=0 \tag{11}$$

$$\frac{\partial w'}{\partial t}+\frac{1}{\rho_0}\frac{\partial p'}{\partial z}-\frac{\theta'}{\bar{\theta}}g=0 \tag{12}$$

$$\frac{\partial u'}{\partial x}+\frac{\partial w'}{\partial z}=0 \tag{13}$$

$$\frac{\partial \theta'}{\partial t}+w'\ \frac{d\,\bar{\theta}}{dz}=0. \tag{14}$$

Next p' is eliminated giving

$$\frac{\partial}{\partial t}\left(\frac{\partial w'}{\partial x}-\frac{\partial u'}{\partial z}\right)-\frac{g}{\bar{\theta}}\frac{\partial \theta'}{\partial x}=0. \tag{15}$$

Then u' and θ' are eliminated giving

$$\frac{\partial^2}{\partial t^2}\left(\frac{\partial^2 w'}{\partial x^2}+\frac{\partial^2 w'}{\partial z^2}\right)+N^2\frac{\partial^2 w'}{\partial x^2}=0 \tag{16}$$

where $N^2=g\frac{d\ln\bar{\theta}}{dz}$ is the bouyancy frequency squared.

Assuming a harmonic wave solution $w'=\mathrm{Re}(Ae^{i\phi})$ where $\phi=kx+mz-\nu t$, and substituting one can solve for the angular frequency, ν. The equation for ν is

$$\nu=\pm\frac{Nk}{(k^2+m^2)^{1/2}}. \tag{17}$$

This gives the phase velocities

$$C_x=\frac{\nu}{k}\ \text{and}\ C_z=\frac{\nu}{m}. \tag{18\&19}$$

and the group velocities

$$U_g=\frac{\partial\nu}{\partial k}=\frac{Nm^2}{(k^2+m^2)^{\frac{3}{2}}}\ \text{and}\ W_g=\frac{\partial\nu}{\partial m}=-\frac{Nkm}{(k^2+m^2)^{\frac{3}{2}}}. \tag{20\&21}$$

From these equations one can see that downward phase propagation, $k>0$, $m<0$ which gives $C_x>0$ and $C_z<0$, gives upward energy propagation, $U_g>0$ and $W_g>0$. The angle between the phase lines and the vertical, α, equals $k/(k^2+m^2)^{1/2}$ which is equal to $\frac{\nu}{N}$. Therefore the tilt of the phase lines depends only on the ratio of the wave frequency to the bouyancy frequency.

TURBULENCE & CRITICAL LEVELS

Internal gravity waves, modified to a greater or lesser extent by shear, are common in the terrestrial atmosphere. They may be traveling relative to the surface of the Earth, having been caused by some transient irregularity such as a thermal, or they may be stationary, appearing as lee waves behind a mountain range or other obstacle (Booker & Bretherton, 1967).

Internal gravity waves propagating with a vertical component of group velocity in a shear flow may encounter critical levels. A critical level is defined as the level at which the horizontal component of phase velocity of the wave is equal to the mean velocity of the fluid normal to the wave front (Booker & Bretherton, 1967). In our case this is when $C_x =$ the horizontal wind speed. For large background Richardson numbers (R>1) gravity waves are almost completely absorbed at critical levels (Booker & Bretherton, 1967). For 1/4<R<1 less complete absorption occurs. Geller et al (1975) found that R<1 appears to be the condition for turbulence.

Our synoptic situation for flights 3-8, with strong westerlies near the tropopause (Lamb,) is such that zonally propagating gravity waves generated near the lower boundary (eg: mountain lee waves) would be expected to encounter a critical level below our measurement level. This is especially true after mid-December when the balloon flights are imbedded in the

stratospheric easterlies (see figure 3). On the other hand, gravity waves with rapid intrinsic phase speeds, such as might be generated by convection, gravity waves propagating meridianally, or gravity waves generated by shear instability or geostrophic adjustment within the stratospheric easterlies might appear in our data.

Mountainous areas produce statistically strong turbulence, and this can be explained by the role played in turbulence generation by stratospheric gravity waves (Barat, 1982). Cadet (1977) accidentally encountered patches of turbulence over a mountainous region while using a constant level balloon to study mean dissipation rates of kinetic energy in the lower stratosphere. Cadet (1977) concluded that gravity waves can vertically transfer significant amounts of energy limited by the dissipation of waves through CAT (clear air turbulence).

Many experiments have been specifically designed to study turbulence and/or find critical levels (Barat, 1982; Larsen et al, 1982; Yamanara & Tanara, 1984; Ruster & Klostermeyer, 1985; and Vincent, 1985). Barat (1982) used highly sensitive balloon borne instruments to make simultaneous and accurate measurements of wind shear, Richardson number, and turbulent intensity. The balloon was equipped with a valve ballast control. It made three oscillations between 14 and 26 mb. Two turbulent layers were observed. One during the first descent, and one during the second ascent. Barat (1982) took Fast Fourier Transforms (FFT's) to get spectral density and found that they exhibit the classical $k^{-5/3}$ power law. Barat (1982) concluded that the balloon follows perfectly the air in which it is embedded, and that turbulent eddies with scales below the balloon diameter give quite negligible contribution to the bobbing motion.

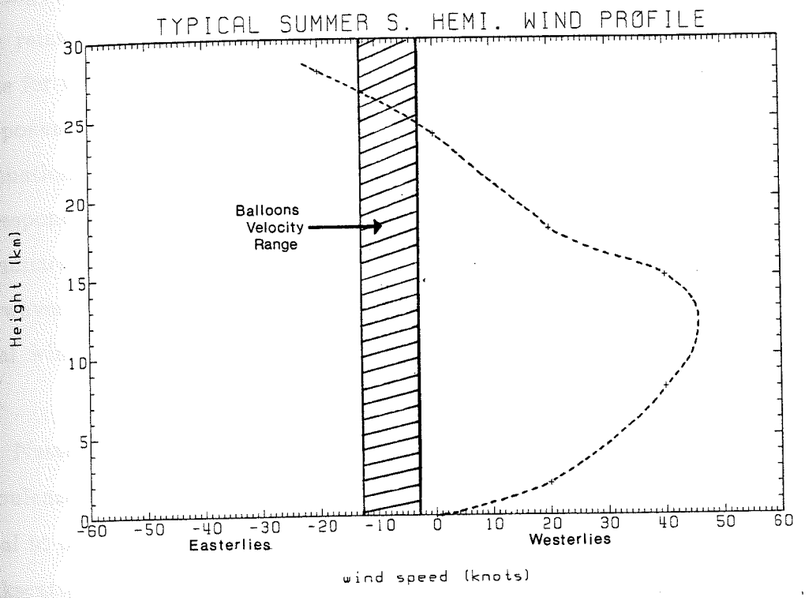

FIGURE 3. Typical geostrophic wind profile with the balloon speed range.

Yamanara and Tanaka (1984) used a zero pressure balloon to examine turbulent layers and zonal wind fluctuations in the stratosphere. The most striking features they found were multiple gust layers of 10-50 m thicknesses with relative wind velocity amplitudes of 1-3 m/sec. They felt a possible cause for the gust layers is a critical-level amplification of the horizontal wind components associated with gravity waves. They also found zonal wind fluctuations with predominant periods of 4 hrs and 1 1/2 hrs, which correspond approximately with zonal wavelengths of 60 and 20 km. Yamanara & Tanaka (1984) felt that these wave-like fluctuations were gravity waves in the mesoscale range. They also found that power spectra of zonal winds throughout the whole mesoscale range exhibited a -5/3 power law.

Nastrom et al (1986) used a doppler radar to measure the refractivity turbulence structure constant, C_n^2. The radar samples turbulence on a scale equal to one-half the radar wavelength therefore C_n^2 is directly related to the backscattered power P_b , according to

$$C_n^2 = K\frac{R^2}{P_t}P_b \tag{22}$$

where P_t is the transmitted power, R is the range, and K is a function of radar operating parameters. Backscattered power is measured on oblique beams, inclined 50^o from the vertical toward the north and east, at approximately 2 km intervals between 4 and 15-20 km. Power spectra of log C_n^2 follow a power law relationship verses frequency with spectral slopes near -5/3 for periods $>$ 2 hrs, and slopes near -1 for periods $<$ 2 hrs (Nastrom et al, 1986).

Gravity waves propagate freely among layers of the atmosphere under a wide variety of conditions, providing a rapid-coupling mechanism. The small

scale turbulence and hence C_n^2 are produced by shears in the background flow, and by gravity waves (Nastrom et al, 1986). Nastrom et al (1986) found a strong correlation between C_n^2, gravity wave activity and background wind.

UNIVERSAL GRAVITY WAVE SPECTRUM

VanZandt (1982) observed that power spectra of mesoscale wind fluctuations exhibit a considerable degree of universality vs season, meteorological conditions, and geographical location. Dewan (1979) and others attributed the horizontal wave number spectra to bouyancy waves while Gage (1979) on the other hand, attributed the spectra to two dimensional turbulence. Both analyses predict a -5/3 slope for the horizontal wave number spectrum.

The spectra of fluctuations observed throughout the oceans and the atmosphere do appear to have many similarities when averaged over suitably large time intervals, suggesting that non-linear wave-wave interactions may act to restore an equilibrium spectrum through a transfer of energy to (from) more (less) energetic components following perturbations due to sources and sinks of wave energy (Fritts, 1984).

Following the Garret and Munk (1975) model for oceanic internal waves, VanZandt (1982) proposed that atmospheric power spectra can be described in terms of a universal spectrum of internal gravity or bouyancy waves. In the oceans the horizontal velocity vs frequency spectra follow a -2 power law, where as in the atmosphere the spectra follow a -5/3 power law (for periods $>$ 10-20 mins). The -5/3 slopes of the horizontal velocity vs frequency spectra lead to the prediction of a -2.4 slope for the horizontal velocity vs vertical wave number spectra (VanZandt, 1982).

A large number of processes contribute to the maintenance and characteristics of the observed gravity wave spectrum in the middle atmosphere. The most obvious of these, perhaps, are the distribution and relative energy of the various tropospheric sources, the filtering and attenuation of the gravity wave spectrum due to propagation in a variable environment, and the evolution of the spectrum due to nonlinear wave-wave and wave-turbulence interactions.

VanZandt et al (1985) looked at spectra derived from mesospheric data taken by the Poker Flat MST radar in support of the STATE experiment during June 1983. The echoing region was between 82 and 90 km. The Garrett and Munk (1975) model for oceanic internal waves was used as the input gravity wave model. VanZandt et al (1985) compared actual power spectral density vs wavenumber data to those predicted by the model. The agreement between the model and the spectra was good enough to support the hypothesis that the mesoscale fluctuations were dominated by gravity waves and that the contribution of 2-dimensional turbulence was small. VanZandt et al (1985) acknowledge that their conclusion holds only for the mesosphere at the time and place of their observations, and that a great deal more work needs to be done before the importance of gravity waves can be fully understood.

Larsen et al (1986) looked at spectra of wind profiles up to heights between 25 and 30 km. Their analysis led to the inference that the vertical velocities follow a -1 slope as a function of frequency and a slope between -1.2 and -1.5 as a function of vertical wave number. The universal gravity wave theory predicts a +1/3 vertical velocity vs frequency slope, and a -2.5 vertical velocity vs vertical wave number slope. Therefore Larsen et al (1986) conclude that their observed spectra do not support the universal gravity

wave predictions, at least to the degree of complexity included in the calculations of Scheffler and Liu (1985).

The situation as it stands, makes it particularly important to obtain observations of spectra of atmospheric variables other than the horizontal velocities. Observations of spectra of the vertical velocity, and other variables such as temperature, are needed to test the universal spectrum predictions, and, if disagreement is found to provide more data for theoretical developments (Larsen et al, 1986).

DATA SET

The data set analyzed in this paper comes from the balloon flights of the EMA (Electrodynamics of the Middle Atmosphere) research project, see Holzworth, 1983. In the first study of it's kind at 26 km, eight small (21.4 m diameter) superpressure balloons were launched from Christchurch, New Zealand in 1983 and 1984. On these flights the temperature and pressure were measured every 40 seconds. These data are the subject of this study.

The temperature was measured with a 10 mil diameter, aluminized bead thermistor, manufactured by the Big Tree Corporation. The temperature output was digitized with an eight bit resolution covering the range from -80 to -40 degrees C (min $\Delta T = 0.16^{o}$). The temperature data are very noisy on the shortest time scales. This is due to limitations resulting from probe placement of the primary instrumentation (vector electric fields). Thermistor beads were mounted on 18 inch booms horizontally extended from the bottom of the main payload body. For a vertical updraft or downdraft this position is frequently in the wake of the balloon, main payload, or electric field booms. Furthermore the payloads were mechanically rotated at 2 rpm (30 sec period) which introduces a beat period between the rotation and the

40 second τ sampling rate. That is, every third T sample is in the same azimuthal location about the load line. Thus we are not confident of the short term temperature data ($\leq$ NBO periods), but the long period averages appear smooth and well behaved.

The pressure was measured with a digital barometer designed at NCAR (National Center for Atmospheric Research). The barometer was designed to be low cost, low power consumption, have a digital output, and to run accurately for unattended periods of up to 1 year (Pike and Bargen, 1976). The pressure sensor consists of a ceramic plate with metalized electrodes, sealed between two Ni-Span-C diaphrams. Capacitance between the internal electrodes and the diaphram increases with applied pressure. The capacitive readout is then digitally encoded to give 16 bit binary output (Pike and Bargen, 1976). The 16 bit encoded pressure data gives a 0.01 mb (0.001 kPa) resolution from 18 to 32 mb, which was the primary operating range.

In most barometers, temperature sensitivity produces the largest systematic errors. If the temperature variation is small, the error may be considered "random", but if the temperature range is large it is necessary to correct for temperature changes (Pike and Bargen, 1976).

Over a moderate pressure and temperature range, the output of the barometer can be computed by the following expression:

$$N = a_o + a_1 P + a_2 T + a_3 TP \tag{23}$$

where N is the digital output; P is the pressure; T is temperature; and a_o, a_1, a_2 and a_3 are constants (Pike and Bargen, 1976). After the constants are determined by a curve fitting process, they can be used to compute the pressure by the inverted form of equation 23:

$$P = \frac{(N - a_o - a_2 T)}{(a_1 + a_3 T)} \tag{24}$$

(Pike and Bargen, 1976). For flights 3-8 the temperature effects were removed from the raw pressure data by Justin Smalley at NCAR, with the use of temperature data from a sensor mounted directly on the digital barometer.

The pressure fluctuation measurement at 21 mb is very sensitive and one can easily see that $\frac{\Delta p}{p} = 0.005$ or equivalently a height variation of 1.2 m (taking the scale height to be 6.65 km).

The telemetry system could store 100 bytes of 40 second pressure and temperature data, giving about 1 hours worth of continuous data for every transmission. It was necessary to have high frequency pressure and temperature data in order to see short period oscillations, such as the neutral bouyancy oscillation. The on-board data were transmitted to the ground through the French ARGOS data collection capability on the TIROS weather satellites (Smalley and Carlson, 1986). Since the satellites were only within transmission range every few hours there are frequent data gaps of half an hour to several hours. These data gaps cause some interesting problems in the analysis of long period waves. For further details on the telemetry system see Powell, 1983.

ANALYSIS

The analysis focuses on flights 4-8. Flights 1 and 2 have not had the temperature effect on the pressure removed however short term pressure variations (e.g. NBO) are still easily identified. Flight 3 lost superpressure very early and therefore moved up and down like a zero pressure balloon instead of floating on a constant density surface. Of the remaining flights about 50% of the data were from intervals long enough to produce useful spectra. Figure 4(a-h) is a plot of the flight trajectories of all eight balloons. It shows

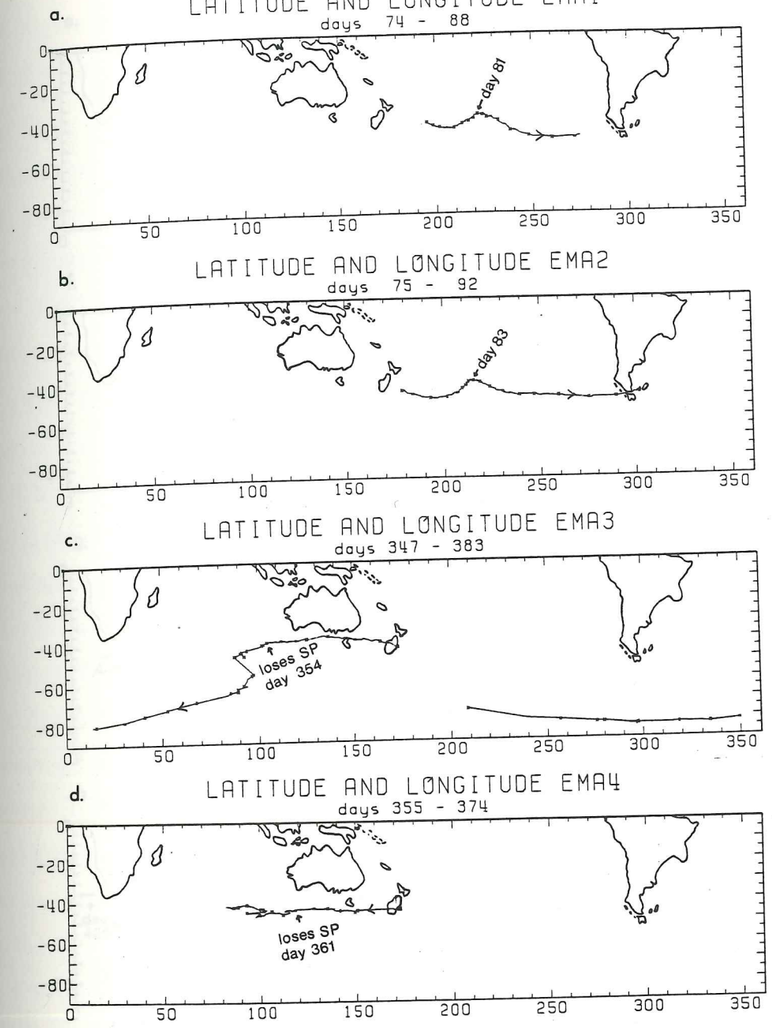

FIGURE 4. Mecator like projections of the flight paths of EMAs 1 - 4. Each * represents one day. (a) Flight path of EMA 1 from 3/15/83 - 3/29/83 (days 74-88). (b) Flight path of EMA2 from 3/16/83 - 4/2/83 (days 75-92). (c) Flight path of EMA3 from 12/13/83 - 1/18/84 (days 347-383). (d) Flight path of EMA4 from 12/21/83 - 1/9/84 (days 355-374).

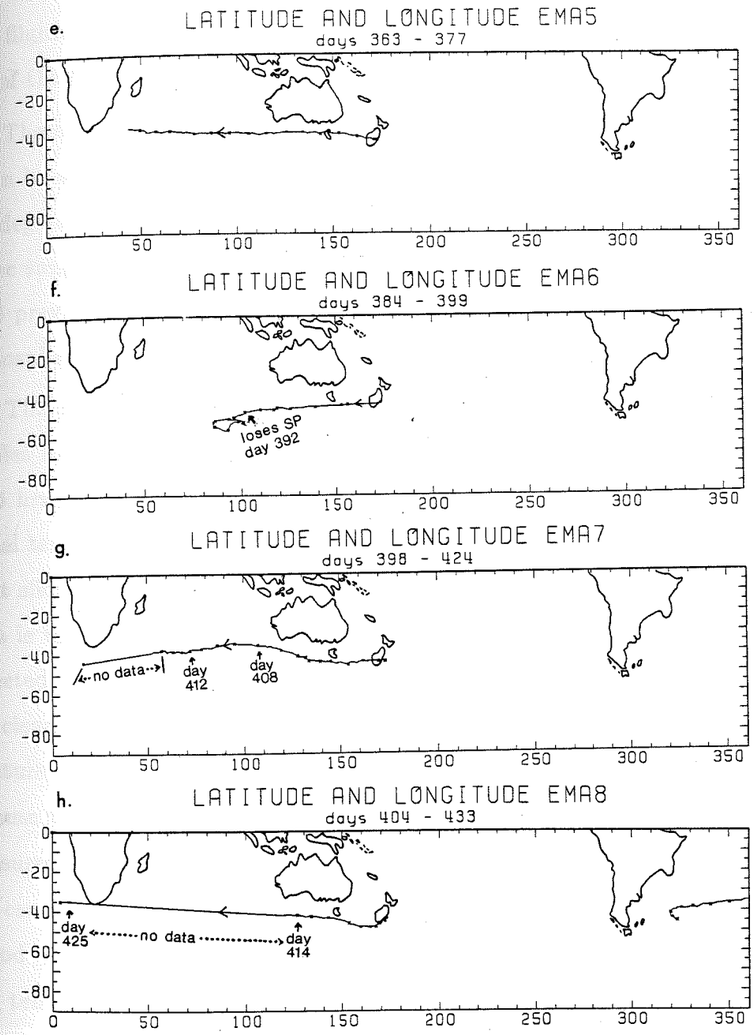

FIGURE 4. continued (e) Flight path of EMA5 from 12/29/83 - 1/12/84 (days 363-377). (f) Flight path of EMA6 from 1/19/84 - 2/3/84 (days 384-399). (g) Flight path of EMA7 from 2/2/84 - 2/28/84 (days 398-424). (h) Flight path of EMA8 from 2/8/84 - 3/8/84 (days 404-433).

that flights one and two travel east with the westerly winter winds, and the rest of the flights travel west with the easterly summer winds.

There is an interesting disturbance present in EMA flights one and two. It can be seen in figures 4a and 4b. The peak of the disturbance moved from 222 degrees on day 81 to 213 degrees on day 83. The westward motion at 5 m/sec suggests that this coherent disturbance was not of tropospheric origin, since previously observed disturbances of tropospheric origin in the southern stratosphere are eastward moving (e.g. Miles & Grose, 1986).

The first step in the analysis was to plot temperature and pressure profiles for all of the flights. Figure 5 is a temperature and pressure profile for 6 hrs of day 361 (Dec 27) of flight number 4. The solid black line is the actual temperature and pressure data with gaps. The dotted line is a twenty point sliding average. One can see that the sense of the low frequency variations is the same. When the pressure increases the temperature increases as expected for a constant density surface. In the pressure measurement one can clearly see the 3.5-4.5 min neutral bouyancy oscillations. Any large temperature jumps (approximately 5% of the data) have already been removed because they are bad data points, yet one can still see that the temperature measurement is much noisier than the pressure. Looking at the average line one can see segments of a small amplitude, quasi-periodic fluctuation with a period of approximately one hour that seems to appear in both the pressure and temperature. Figures 6, 7, and 8 are examples of the temperature and pressure profiles from flights 5, 7, and 8. Similar features can be seen in these figures.

From the real time data, we can experimentally determine the local lapse rate by looking at time periods when the balloon had not yet reached superpressure, or had lost superpressure. When a balloon is superpressured,

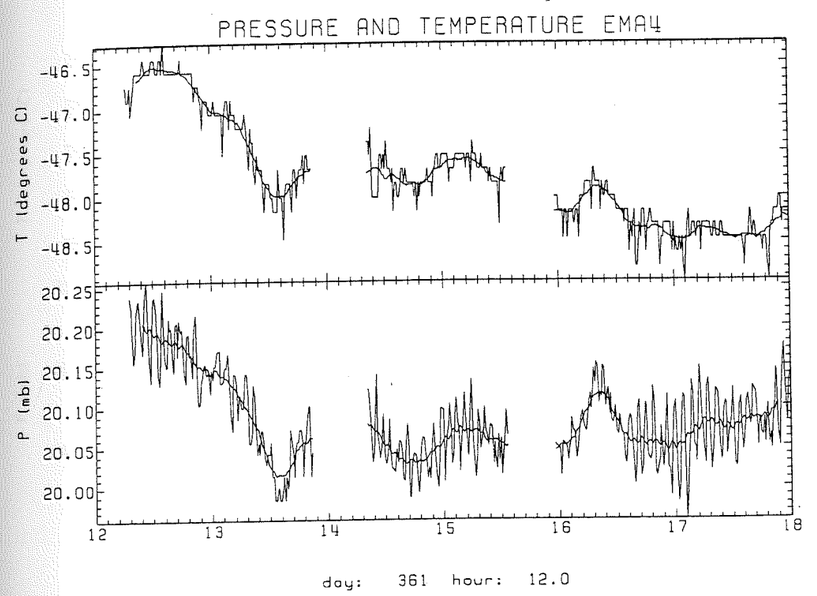

FIGURE 5. Pressure and temperature data from flight #4, Dec. 27, 1983 (day 361), hours 12-18. The solid line through the middle of the data is a 20 point sliding average.

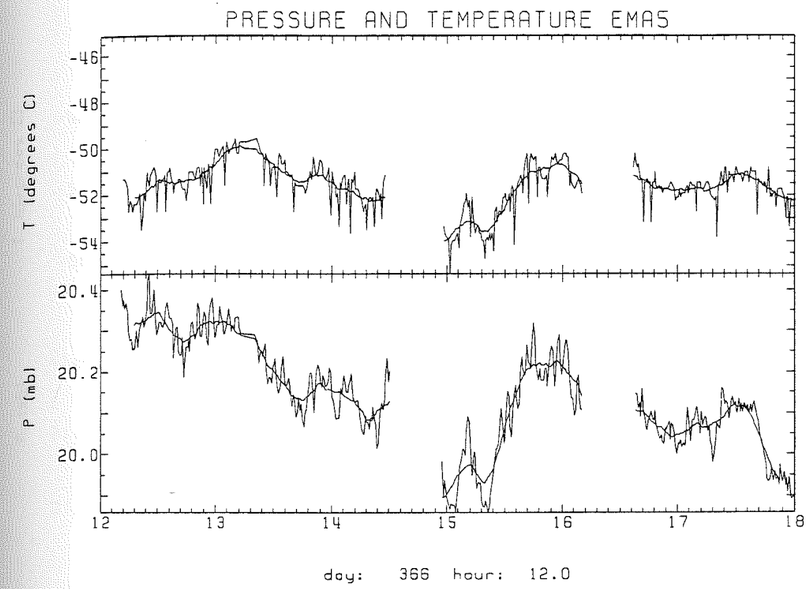

FIGURE 6. Pressure and temperature data from flight #5, Jan. 1, 1984 (day 366), hours 12-18. The solid line through the middle of the data is a 20 point sliding average.

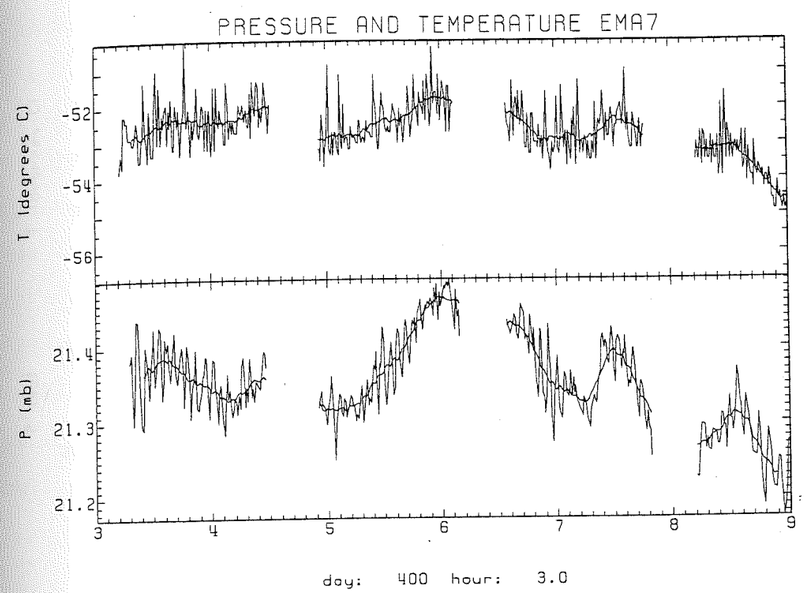

FIGURE 7. Pressure and temperature data from flight #7, Feb. 4, 1984 (day 400), hours 3-9. The solid line through the middle of the data is a 20 point sliding average.

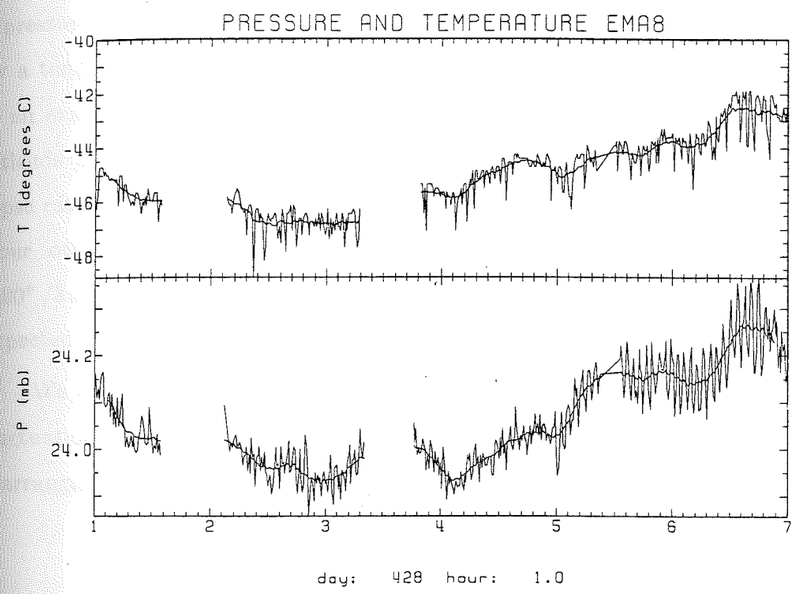

FIGURE 8. Pressure and temperature data from flight #8, March 3, 1984 (day 428), hours 1 - 7. The solid line through the middle of the data is a 20 point sliding average.

the sense of the pressure and temperature variations is the same such that the density remains constant. During non-superpressure times the balloon motion is governed by variable bouyancy forces related to balloon volume so a pressure decrease resulting from an upward balloon motion is accompanied by a temperature increase due to the positive lapse rate at 26 km. Figure 9 is an example of such a pressure and temperature change. Calculating the altitude change from the pressure change one can calculate an approximate lapse rate. For the example in figure 9 the calculated lapse rate is 1.85^o /km. Four other such calculations for different flights gave numbers between 1.20^o /km and 1.51^o /km. These numbers are in good agreement with the expected 1 to 2^o /km lapse rate at 26 km (Holton, 1979).

We can calculate the density ρ by looking at pressure and temperature fluctuations during superpressure periods. Assuming the ideal gas law, and rearranging we get

$$\rho = \frac{1}{R}\frac{\Delta P}{\Delta T} = 0.348\left(\frac{\Delta Pmb}{\Delta T^o K}\right) kg\ /m^3. \tag{25}$$

At 26 km we expect a value of ρ around 0.036 kg/m^3 (Holton, 1979). For ten random samples with $\Delta P \geq 0.1$ mb for flights 5 - 8 calculated values of ρ ranged between 0.0316 kg/m^3 and 0.0493 kg/ m^3 . The error in calculation is $\pm 0.008 kg\ /m^3$. Five of the ten values are within ± 0.004 of the expected value, and 80% are within the calculated error range. These calculations lead to the conclusion that the balloons do in fact float on a constant density surface.

In most of the data it is difficult to see the coherence of the small amplitude fluctuations because of the data gaps. Figure 10 is an example of what appears to be a coherent wave decreasing in amplitude. In the temperature we can clearly see the wave amplitude decrease from two degrees to almost

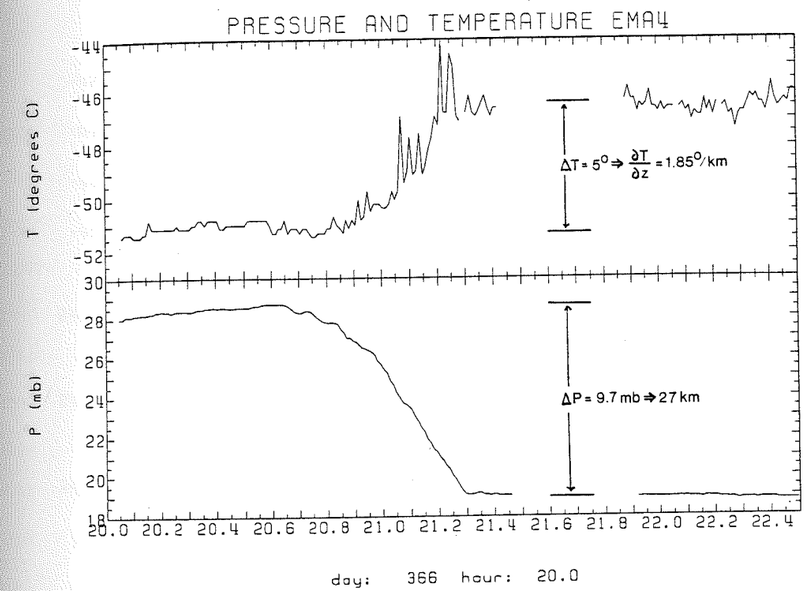

FIGURE 9. Pressure and temperature profile from flight #4, day 366 showing a non-superpressure pressure and temperature change with lapse rate calculation.

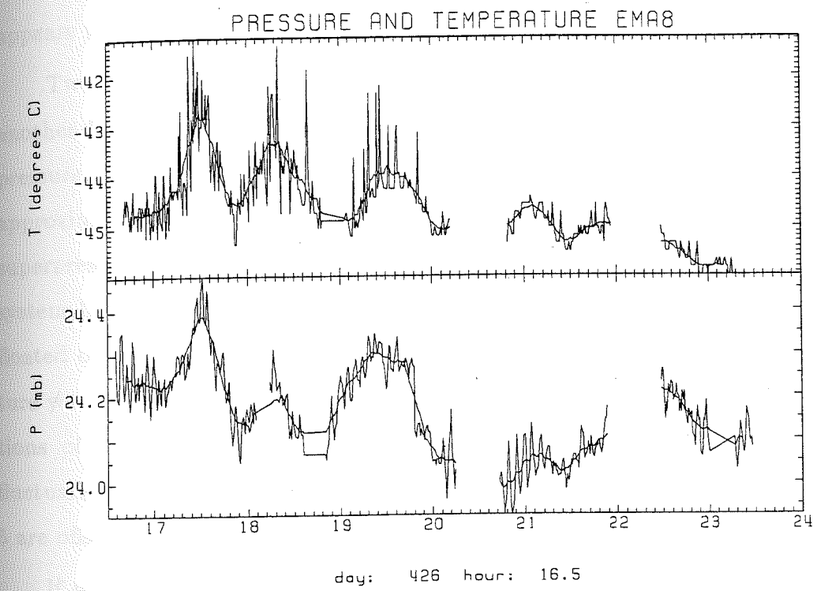

FIGURE 10. Example of wave amplitude decreasing with time from flight #8, day 426.

no fluctuation in approximately 6 hours. The decrease is less obvious in the pressure which has had linear trends of greater than half an hour removed. This amplitude decrease could be a wave damping out. The damping rate appears to be 10 to 15 % per hour.

Two balloons, EMAs 4 and 5, came very close (within $\approx$ 200 km) to one another for a short time. By that time in it's flight EMA 4 had lost superpressure and was floating at the 18 mb level during the day only. This is approximately 400 m higher than EMA 5 since the extra gas providing the superpressure which acted as a load no longer existed, making the EMA 4 system lighter. Since EMA 4 was no longer superpressured at night it only floated on a constant density surface during the day when the gas temperature was high enough to fully inflate the balloon. There are only a few variations of large enough scale to compare. Figure 11 is one example of a fluctuation of similar sense in both EMAs 4 and 5. In figure 11 EMAs 4 and 5 are offset by 12 minutes.

If we were to assume that the similar fluctuations in figure 11 were due to a wave with wave vector parallel to the line between EMAs 4 and 5, we would conclude that the horizontal wavelength was greater that 466 km (the separation distance at the time in fig 11). However, we cannot assume the wave is propagating from one balloon to the other because a 12 minute lag over a 466 km distance gives a phase speed greater than the speed of sound. Typical motions of gravity waves in the atmosphere have been seen to have horizontal wavelengths of 10 to 10^3 km, periods of 10 to 10^3 min, phase speeds of 10 to 10^2 m/sec, and vertical scales of $\geq$ 10 km (Fritts, 1986). Since the balloons are only separated 400 m vertically and other waves have been seen with horizontal wavelenghts on the order of the distance between the balloons, we can suggest the possibility that EMAs 4 and 5 are seeing the

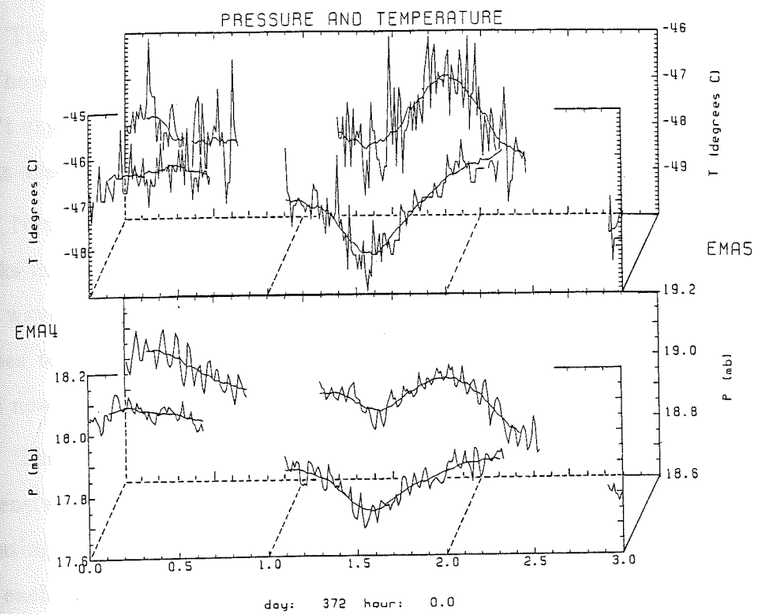

FIGURE 11. Pressure and temperature profiles of EMAs 4 and 5 superposed.

same disturbance, with 12 minutes being the phase difference of observations on a large scale wave front.

The balloons' horizontal velocity is approximately 5 m/sec (15 ± 10 km/hour). Since we expect most waves to be traveling much faster, we don't expect much problem from doppler shifting, but we are not sure exactly what effect it might have.

Next we preformed a spectral analysis on the data. We were looking for peaks in the > 10 minute range that might possibly be attributable to gravity wave activity. We also wanted to compare our spectra and spectral slopes to those of previous studies to check for corroboration as well as to add new data to the subject.

The spectral analysis proved to be rather challenging because of the extensive data gaps. Instead of attempting to fill the gaps, and possibly creating artificial peaks, it was decided to run a FFT (fast Fourier transform) on each individual section of data. The individual sections were then averaged to give daily averages.

Following Brault and White (1971) each section of data was set to have zero mean and linear trends were removed. Zero's were appended if necessary to make the data set of length 2^n points. A cosine bell window was then applied to the first and last 10% of the data. The data were then Fourier transformed using a routine written by R.C. Singleton (1968). The input to the routine was n - the number of data points, r - an n point array of the real part of the data vector, and i - an n point array of the imaginary part of the data vector to be transformed. In the case of our data, the input imaginary array is equal to zero. The output of the routine contains two n point arrays of the real and imaginary parts of the transformed sequence.

Next the power spectrum is calculated from the real and imaginary transformed values $\tilde{r}$ and $\tilde{i}$ respectively. The power $P(s_k)$ at frequency s_k is given by

$$P(s_k) = (\tilde{r}(s_k)^2 + \tilde{i}(s_k)^2)\left(\frac{n}{n - \#zeros}\right) \tag{26}$$

where

$$s_k = \frac{k-1}{n\,\Delta x},\ k = 1,2,3 \ldots n. \tag{27}$$

For our data Δx is 40 seconds or 463 microdays, and n is either 128 or 256 points (85 or 170 minutes, respectively).

Figure 12 is an example of the power spectrum of an individual 85 minute section of pressure data. It is plotted on a log-log scale and we can see the NBO at around 4.5 minutes. Figures 13-15 are examples of daily averages of spectra. The NBO is clear in the pressure spectrum of almost all plots. In figure 13 the NBO is a distinct peak, but in most of the spectra the NBO covers a range from approximately 3 to 4.5 mins. The width of the NBO seems to be due to the averaging, and an occasional phase shift in the NBO. Note that the temperature spectra is cut off at 5.7 minutes to eliminate confusion due to the noise in the high frequency range.

It is difficult to see waves greater than the NBO period in the spectra because of the limit on frequency due to the shortness of the data sections. Approximately 95% of the FFTs used 128 points, which corresponds to 1.4 hrs of data. Each FFT results in a power spectrum with periods from 1.42 hrs to 1.35 mins, but with very few points in the >10 minute range, making it unlikely that we could resolve many peaks there.

Approximately 5% of the data sets were long enough to compute 256 point FFTs. These resulted in a few more points in the low frequency range

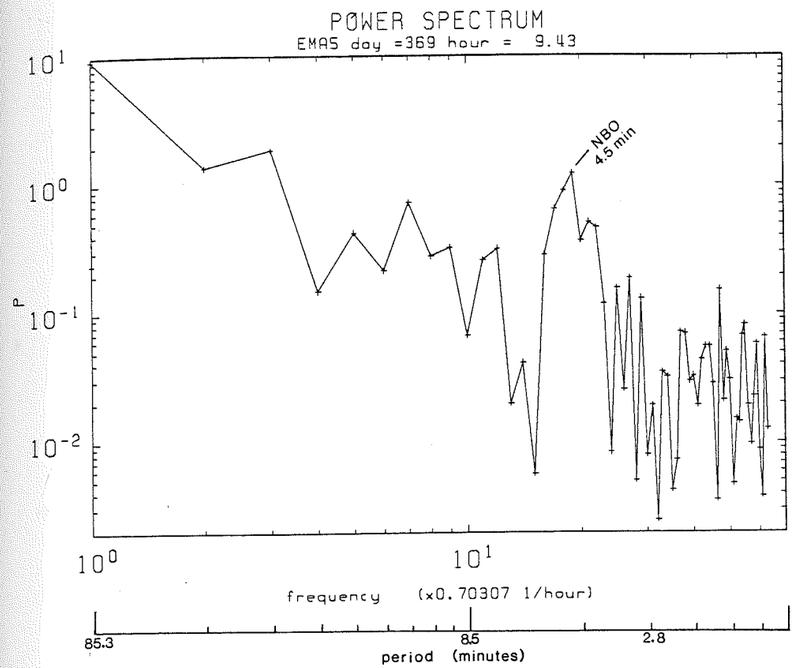

FIGURE 12. Pressure power spectrum from a single 128 point data section of flight #5 day 369. Note the log-log scale.

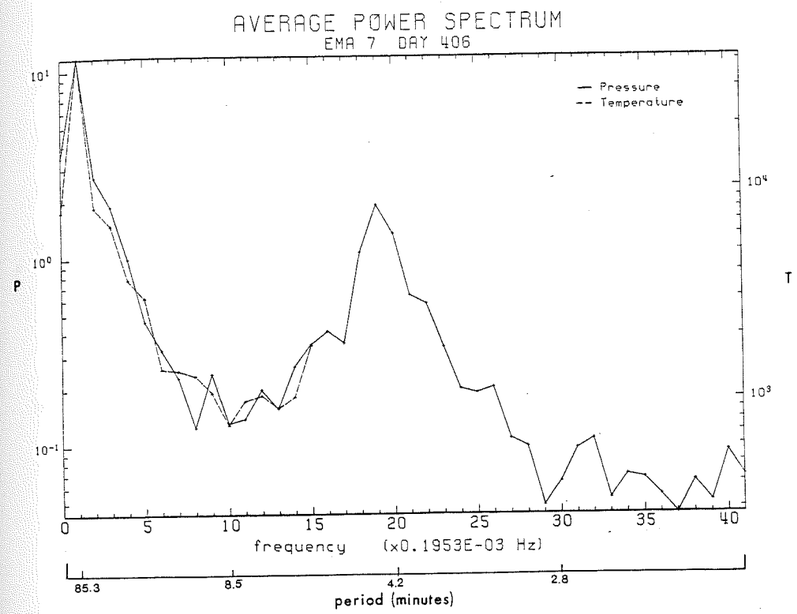

FIGURE 13. Average power spectrum of flight #7, Feb. 10 (day 406). The pressure power scale is on the left and corresponds to the solid line. The temperature power scale is on the right and corresponds to dotted line.

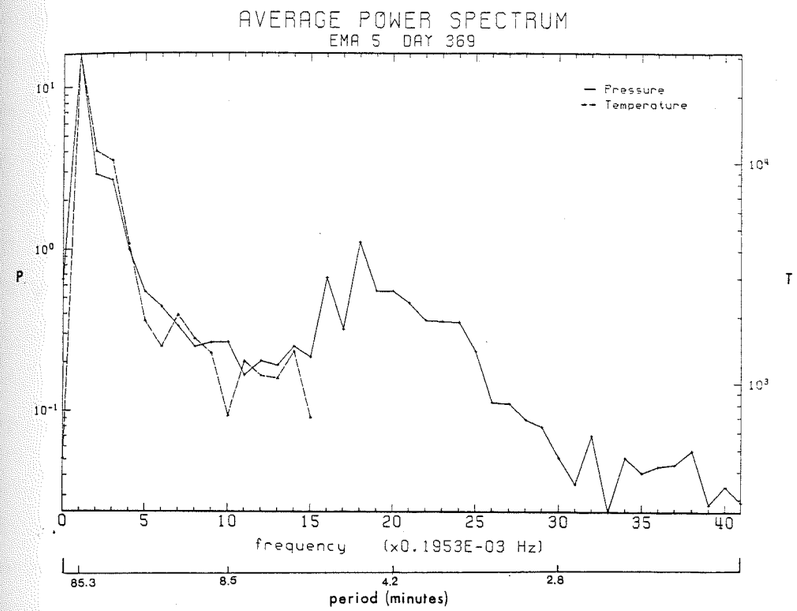

FIGURE 14. Average power spectrum of flight #5, Jan. 4 (day 369).

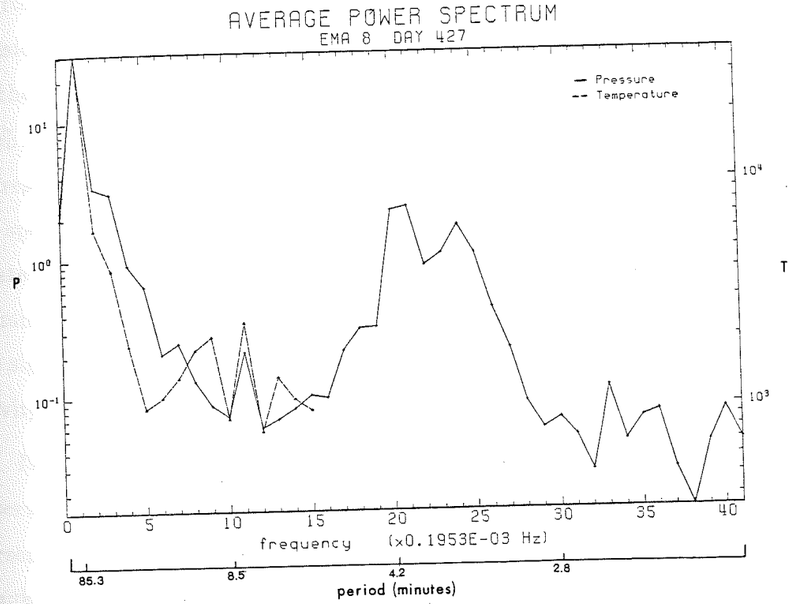

FIGURE 15. Average power spectrum of flight #8, March 2 (day 427).

giving a better possibility of seeing peaks greater than the NBO. Figures 16 and 17 are the averages of 256 point FFTs from flight number 7. Figure 16 is from day 403 (Feb. 7). Five overlapping 256 point sections were transformed and averaged together. There is a peak at 28.4 mins and another at 12.2 minutes. These peaks are not statistically significant at the 80 % confidence level, yet they appear again in the next example. The NBO is present in the pressure, yet not as distinctly as in some of the other average spectra. Figure 17 is the average of all sections of data from flight 7 with greater than 256 points (20 sections). Once again there are peaks at 28 and 12 minutes. There are also peaks at 9 and 7 minutes. Some of these peaks are significant at the 80 % confidence level. These peaks could be due to gravity wave activity.

Next we looked at stormy days during the flights. Many people have observed gravity waves during severe weather (Bowhill & Gnanalingam, 1985; Larsen et al, 1982; and Lu et al, 1985). Larsen et al (1982) found that when clouds developed sufficiently in height to reach the tropopause, gravity wave oscillations in vertical velocity above the troposphere would develop. Bowhill & Gnanalingam (1985) also found a clear correlation between increased gravity wave activity in the stratosphere (12 - 24 km) and cloud tops exceeding 20,000 feet.

Lu et al (1985) further examined the relationship between internal gravity waves and thunderstorms. They felt the two important aspects to investigate were first, that some thunderstorm cells could be initiated or excited by propagating gravity waves, and second, that thunderstorms could contribute to the energy of the atmospheric gravity wave field. Lu et al (1985) concluded that only strong overshooting cells could contribute to thunderstorm generated gravity waves in the stratosphere, and that much more work

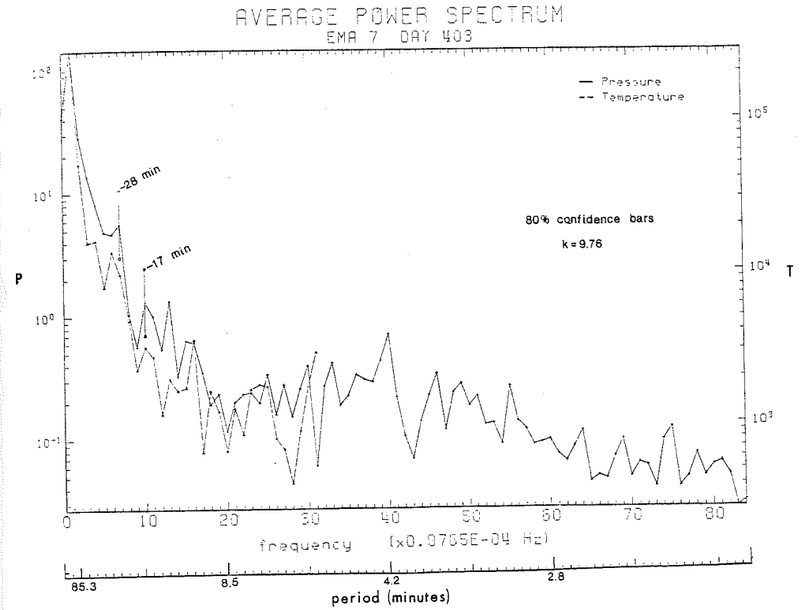

FIGURE 16. 256 point average power spectrum for flight #7, Feb. 7 (day 403).

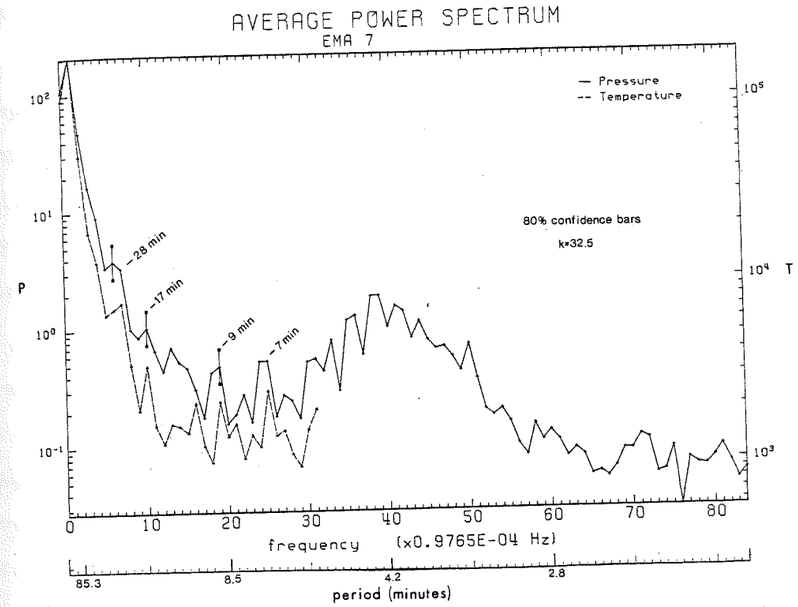

FIGURE 17. 256 point average power spectrum of all the flight #7 sections with $>$ 200 points.

needs to be done. However, it was very clear from their data that in the troposphere the spectra for thunderstorm active periods were much stronger than for quiet periods.

In order to confirm that severe weather leads to stronger spectra we compared the strength of the calculated pressure and temperature spectra to location and weather. The balloon payloads included a lightning counter as well as a measure of the down-looking background dc light, so it is relatively easy to tell when it is cloudy below the balloon and when there is an active thunderstorm nearby (see also Holzworth et al, 1986).

Figures 18 & 19 are histograms of the distribution of pressure and temperature spectra in the highest 10 percent of total power for flights 5 and 7. For flight 5, days 369-375, the only stormy day was day 369. From our analysis we cannot conclude that the power on day 369 was significantly stronger than on any of the other days. It is possible that the storm was too low for the thunderstorm generated gravity waves to reach the balloon. Figure 19 for flight 7 shows enhanced power from days 401-405 and on days 408 and 412. Days 408 and 412 were very cloudy days, so the enhanced power on these days is expected. Days 401-405 correspond to when the balloon was south of Australia as seen in figure 4g. It is possible that the enhanced power is due to lee waves generated by flow over Australia although we wouldn't expect lee waves to reach the balloon's 26 km altitude. Possibly wave activity was enhanced by turbulence due to lee waves reaching critical levels.

The next step in the analysis was to exponentially fit the power spectra for determination of the power law, and comparison with other work. The slope of the power spectra appears to change near the 20 min period point which is similar to the 20-25 min intersection point of Larsen et al (1986) and others. Because of the uncertainty in the short period part of the spectra,

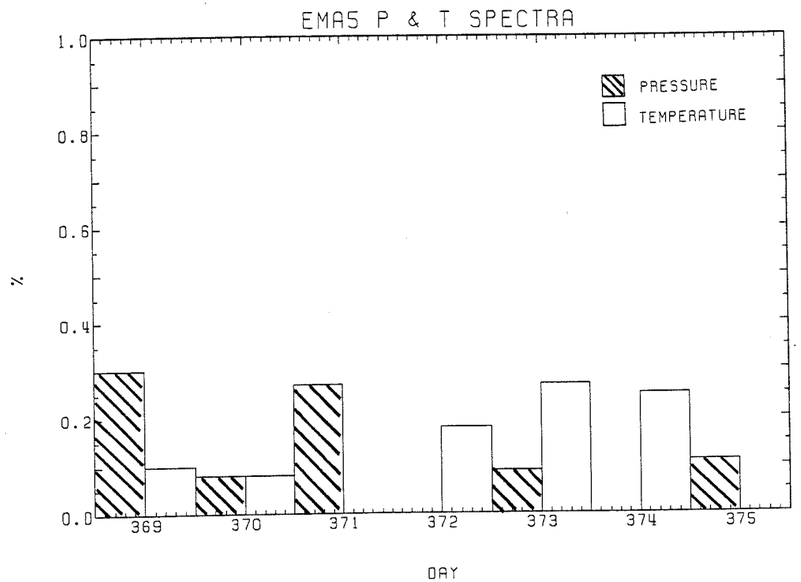

FIGURE 18. Histogram of the percent of power spectra for each day of flight #5 in the highest 10 percent.

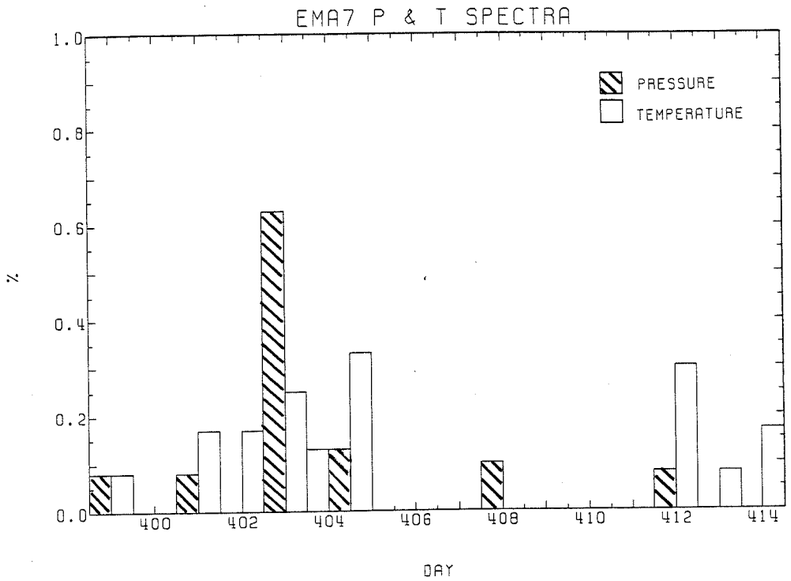

FIGURE 19. Histogram of the percent of power spectra for each day of flight #7 in the highest 10 percent.

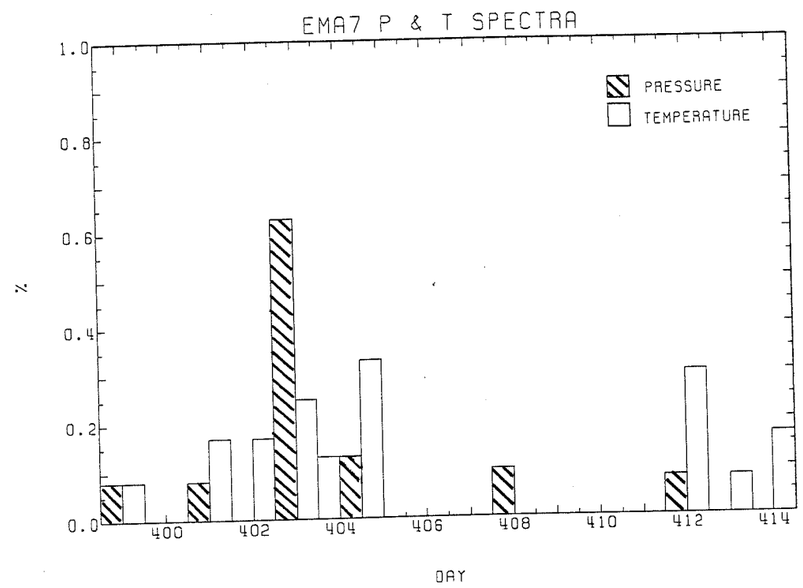

FIGURE 19. Histogram of the percent of power spectra for each day of flight #7 in the highest 10 percent.

due to the NBO fluctuation, only the first 6-10 points are fit. Therefore, the focus of our attention is on the portion of our spectra in the mesoscale ($\approx$ 20 minutes - 3 hours) range.

Previous calculations of pressure spectra have been performed by Gossard (1960), Herron et al (1969), and recently by Canavero and Einaudi (1986). All these measurements were made at the ground using microbarographs. Gossard (1960) found the power law for pressure/frequency spectra to be typically -2, and Canavero and Einaudi found a power law of -7/3. Temperature spectra have been calculated by Kao (1970), Mantis and Pepin (1971), and recently by Nastrom and Gage (1986). Kao (1971) found a -3 temperature/wave number slope, and a -1 temperature/frequency slope in the mesoscale range, and Nastrom and Gage (1986) found a -5/3 temperature/wave number slope.

Two mechanisms have been suggested to be responsible for the observed mesoscale spectra. The first is strongly nonlinear and can be categorized as quasi-two-dimensional turbulence. The second is weakly nonlinear and involves a spectrum of internal bouyancy waves.

Our pressure spectra approximately follow a -7/3 slope with frequency, in good agreement with Canavero and Einaudi (1986), and our temperature spectra approximately follow a -5/3 slope with frequency, in good agreement with wave number spectra calculated by Nastrom and Gage (1986).

Figure 20 is a plot of the slopes and standard deviations obtained using a modified line fitting routine by Bevington (1969). For flight 5 the slopes of the pressure spectra range between -2.51 and -1.80 with an average of -2.11, and the slopes of the temperature spectra range between -1.47 and -1.88 with an average of -1.66. Similarly flight 7 has pressure slopes between -2.47 and -1.82 with an average of -2.18, and temperature slopes between -2.27 and

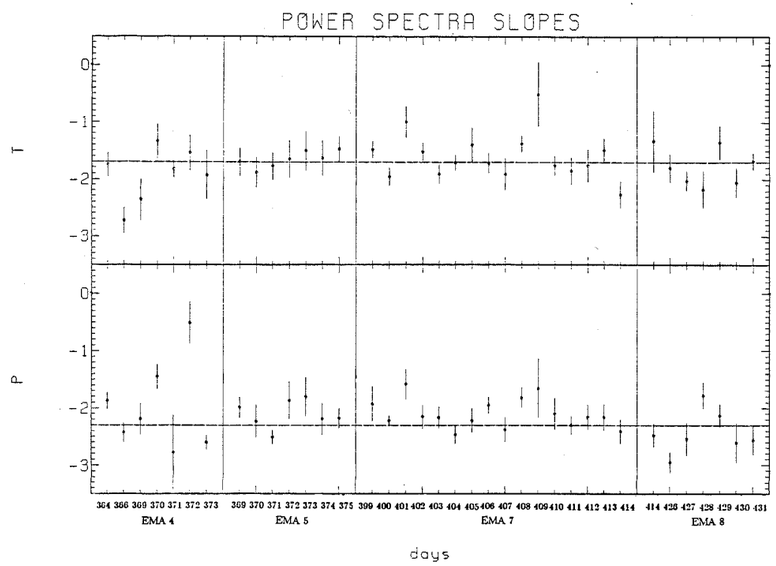

FIGURE 20. Pressure and temperature power spectral slopes for all the days analyzed. The dotted line is the -1.7 average slope for temperature, and the -2.3 average slope for pressure.

-1.38 with an average of -1.72. Flight 8 produced steeper less consistent slopes. Slopes of pressure spectra range from -1.78 to -2.95 with an average of -2.71, and temperature spectra range from -1.33 to -2.16 with an average of -1.94.

The average pressure/frequency slope for flights 5-8 is -2.30 ±0.24, and the average temperature/frequency slope is -1.76 ±0.26. Turbulence theory predicts a -5/3 slope for temperature/frequency spectra, and a steeper -7/3 slope for pressure/frequency spectra (Lumley and Panofsky, 1964). VanZandt's theory predicts a -5/3 slope for both temperature and pressure spectra according to Canavero and Einaudi (1986). It is not clear if these predicted slopes are for frequency or wave number spectra, and how the spectra are expected to change from the wave number to the frequency domain.

It is clear that more theoretical work needs to be done to distinguish between the 2-D turbulence and universal gravity wave spectrum theories. As Canavero and Einaudi (1986) have pointed out, surface data show similar pressure spectral shapes for different time periods, but varying energy levels. These superpressure balloon data show similar non-stationarity, so they do not support the concept of a truly universal gravity wave spectrum.

CONCLUSIONS

As expected from the climatology of the region the first two flights (EMAs 1 & 2) move west to east in a very regular fashion, and the summer flights (EMAs 3-8) move east to west. Except when they leave the constant density surface, there is generally no lateral motion that can be detected within the relatively low resolution of the positioning data, hence, no evidence for large scale 2-D turbulence or large scale inertial oscillations. An exception was a weak disturbance observed on EMAs 1 and 2 near -40

latitude, 220 longitude that was apparently moving westward at $\approx$ 5 m/sec. This westward motion is inconsistent with tropospheric origin for the disturbance.

Two distinct types of fluctuations can be seen in the raw temperature and pressure data. The first is the expected, and well documented neutral bouyancy oscillation with a period of around four minutes which also demonstrates the instrumental sensitivity. The second is characterized as a small amplitude fluctuation with periods between 0.1 and 1 hour.

Using data from non-superpressured times, the lapse rate was calculated to be from 1.2°/km to 1.8°/km in good agreement with the expected value at 26 km. Also, as expected, the density was found to be fairly constant, even during significant pressure and temperature fluctuations, with values around 0.036 kg/m^3, indicating that the balloons did follow a constant density surface.

In most of the data it is difficult to see the coherence of the one hour fluctuations because of their small amplitude and the data gaps. An interesting exception is the example a wave damping out with a damping rate of approximately 10 to 15 % per hour.

During a few days EMAs 4 and 5 flew fairly close together. Since the two balloons were almost 500 km apart, in order for them to see the same wave at almost the same time, the horizontal wavelength would have to be at least 500 km. However, for the remainder of the simultaneous data no obvious fluctuations were the same for any pair of payloads.

Spectral analysis of the data clearly showed the NBO in almost all cases. In the average spectra, the NBO was seen as a wide peak due to frequent phase shifts. Few peaks at frequencies below NBO were observed because of the limitation placed on the spectra due to the shortness of the data sections.

An exception to this was in the case of the few longer spectra that were performed. Here a few peaks were present in the greater than 10 minute range, and peaks were also seen around 9 and 7 minutes. All spectral averages indicate that the majority of the power is in the long period range.

No obvious correlation was found between cloudiness and enhanced power, although there were not enough cloudy days in the data set for an extensive or conclusive study. Note, however that nearly all of the data were taken over the southern hemisphere oceans where intense convective activity was relatively rare.

Calculation of power spectral slopes showed that pressure spectra on the average follow a -7/3 power law, and temperature spectra on the average follow a -5/3 power law. Both average slopes are in good agreement with spectral slopes predicted by turbulence theory. The temperature is also in good agreement with VanZandt's universal gravity wave spectrum theory, however the pressure spectra disagrees. It is not clear how the quasi-Lagrangian balloon coordinates affect the results. With further analysis of the data set, it may be possible to more clearly distinguish between these two theories.

REFERENCES

Barat, J., 1982. Some characteristics of clear air turbulence in the middle stratosphere. *J. Atmos. Sci.,* **39,** 2553-2564.

Beer, T., 1972. *Atmospheric Waves,* John Wiley, New York.

Bevington, P.R., 1969. *Data Reduction and Error Analysis for the Physical Sciences.* McGraw-Hill, New York.

Booker, J.R., and Bretherton, F.P., 1967. The critical layer for internal gravity waves in a shear flow. *J. Fluid Mech.,* **27,** 513-539.

Bowhill, S.A., and Gnanalingam, S., 1985. Gravity waves in severe weather. *Handbook for MAP,* **18,** 128-135, SCOSTEP Secretariat, Univ. IL, Urbana.

Brault, J.W., and White, O.R., 1971. The analysis and restoration of astronomical data via the fast Fourier transform. *Astron. and Astrophys.,* **13,** 169-189.

Cadet, D., 1977. Energy dissipation within intermittent clear air turbulence patches. *J. Atmos. Sci.,* **34,** 137-142.

Cadet, D., 1978. The superpressure balloon sounding technique for the study of atmospheric meso- and microscale phenomena. *Bull. Amer. Meteor. Soc.,* **59,** 1119-1127.

Canavero, F.G., and Einaudi, F., 1986. Time and space variability of spectral estimates of atmospheric pressure. *J. Atmos. Sci.,* in press.

Dewan, E.M., 1979. Stratospheric wave spectra resembling turbulence. *Science,* **204,** 832-835.

Fritts, D.C., 1984. Gravity wave saturation in the middle atmosphere: a review of theory and observations. *Rev. Geophys. and Space Phys.,* **22,** 275-308.

Fritts, D.C., 1986. Gravity waves in the middle atmosphere: recent progress and needed studies. *Handbook for MAP,* **18,** SCOSTEP Secretariat, Univ. IL, Urbana.

Fritts, D.C., and Rastogi, P.K., 1985. Convective and dynamical instabilities due to gravity wave motions in the lower and middle atmosphere: theory and observations. *Radio Sci.,* **20,** 1247-1277.

Gage, K.S., 1979. Evidence for a -5/3 law inertial range in mesoscale two-dimensional turbulence. *J. Atmos. Sci.,* **36,** 1950-1954.

Garrett, C., and Munk, W., 1975. Space-time scales of internal waves: a progress report. *J. Geophys. Res.,* **80,** 291-297.

Geller, M.A., Tanaka, H., and Fritts, D.C., 1975. Production of turbulence in the vicinity of critical layers for internal gravity waves. *J. Atmos. Sci.,* **32,** 2125-2135.

Gossard, E.E., 1960. Spectra of atmospheric scalars. *J. Geophys. Res.,* **65,** 3339-3351.

Gossard, E., and Hooke, W., 1975. *Waves in the Atmosphere,* Elsevier Sci. Pub. Co., New York.

Herron, T.J., Tolstoy, I., and Kraft, D.W., 1969. Atmospheric pressure background fluctuations in the mesoscale range. *J. Geophys. Res.,* **74,** 1321-1329.

Hines, C.O., 1960. Internal gravity waves at ionospheric heights. *Can. J. Phys.,* **38,** 1441-1481.

Holton, J.R., 1979. *An Introduction to Atmospheric Meteorology,* Academic Press, Inc., San Francisco.

Holton, J.R., 1982. The role of gravity wave induced drag and diffusion in the momentum budget of the mesosphere. *J. Atmos. Sci.,* **39,** 791-799.

Holzworth, R.H., 1983. Electrodynamics of the stratosphere using 5000 m^3 superpressure balloons. *Adv. Space Res.,* **3,** 107-114.

Holzworth, R.H., Norville, K.W., Kinter, P.M., and Powell, S.P., 1986. Stratopsheric conductivity variations over thunderstorms. *J. Geophys. Res.,* **91,** 13257-13263.

Houghton, J.T., 1978. The stratosphere and mesosphere. *Q. J. R. Meteor. Soc.,* **104,** 1-19.

Kao, S.K., 1970. Wavenumber-frequency spectra of temperature in the free atmosphere. *J. Atmos. Sci.,* **27,** 1000-1007.

Lally, V.E., 1975. Scientific Ballooning Handbook. *NCAR Tech. Note IA-99,* Atmospheric Tech. Div., Boulder, Co.

Lamb, H.H., 1972. *Climate: Present, Past, Future.* Vol. 1, Methuen & Co. LTD, London.

Larsen, M., Kelley, M., and Gage, K., 1982. Turbulence spectra in the upper troposphere and lower stratosphere at periods between 2 hrs and 40 days. *J. Atmos. Sci.,* **39,** 1035-1041.

Larsen, M., and Swartz, W.E., 1982. Gravity wave generation by thunderstorms observed with a vertically-pointing 430 MHz radar. *Geophys. Res. Letters,* **9,** 571-574.

Larsen, M.F., Woodman, R.F., Sato, T., and Davis, M.K., 1986. Power spectra of oblique velocities in the troposphere and lower stratopshere observed at Arecibo, Puerto Rico. *J. Atmos. Sci.* **42,** in press.

Levanon, N., Oehlkers, R., Ellington, S., Massman, W., and Suomi, V., 1974. On the behavior of superpressure balloons at 150 mb. *J. Applied Meteor.,* **13,** 494-504.

Lindzen, R.S., 1981. Turbulence and stress owing to gravity wave and tidal breakdown. *J. Geophys. Res.,* **86,** 9707-9714.

Lu, D., VanZandt, T.E., and Clark, W.L., 1985. Observation and analysis of thunderstorm generated gravity waves in the lower stratosphere. *Handbook for MAP,* **18,** 220-225, SCOSTEP Secretariat, Univ. IL, Urbana.

Lumley, J.L., and Panofsky, H.A., 1964. *The Structure of Atmospheric Turbulence.* J. Wiley & Sons, New York.

Mantis, H.T., and Pepin, T.J., 1971. Vertical temperature structure of the free atmosphere at mesoscale. *J. Geophys. Res.,* **76,** 8621-8628.

Massman, W.J., 1978a. On the nature of vertical oscillations of constant volume balloons. *J. Applied Meteor.,* **17,** 1351-1356.

Miles, T., and Grose, W.L., 1986. Transient medium-scale wave activity in the summer stratosphere. *Bull. Amer. Meteor. Soc.,* **67,** 674-686.

Morel, P., and Bandeen, W., 1973. The EOLE experiment: early results and current objectives. *Bull. Amer. Meteor. Soc.,* **54,** 298-305.

Nastrom, G.D., and Gage, K.S., 1986. A climatology of atmospheric wavenumber spectra of wind and temperature observed by commercial aircraft. *J. Atmos. Sci.,* **42,** 950-960.

Nastrom, G.D., Gage, K.S., and Ecklund, W.L., 1986. Variability and turbulence, 4-20 km, in Colorado and Alaska from MST radar observations. *J. Geophys. Res.,* **91,** 6722-6734.

Pike, J.M., and Bargen, D.W., 1976. The NCAR digital barometer. *Bull. Amer. Meteor. Soc.,* **57,** 1106-1111.

Powell, S.P., 1983. An on-board microprocessor system for precessing electric field signals on superpressure balloons. Masters Thesis, Electrical Engineering Department, Cornell University.

Richter, J.H., 1969. High resolution tropospheric radar sounding. *Radio Sci.,* **4,** 1261-1268.

Ruster, R., and Klostermeyer, J., 1985. Instabilities and turbulence at mesospheric heights as observed by VHF radar. *Handbook for MAP,* **18,** 216-219, SCOSTEP Secretariate, Univ. IL, Urbana.

Scheffler, A.O., and Liu, C.H., 1985. On observation of gravity wave spectra in the atmosphere by using MST radars. *Radio Sci.,* **20,** 1309-1322.

Singleton, R.C., 1969. An algol convolution procedure based on the fast Fourier transform. *Comm. ACM,* **12,** 179-184.

Smalley, J.H., and Carlson, N.E., 1986. A long duration balloon system for middle atmosphere measurements. *COSPAR Sumposium 10,* in press.

TWERLE Team, 1977. The TWERLE experiment. *Bull. Amer. Meteor. Soc.,* **58,** 936-948.

VanZandt, T.E., 1982. A universal spectrum of bouyancy waves in the atmosphere. *J. Geophys. Res.,* **9,** 575-578.

VanZandt, T.E., 1985. A model of gravity wave spectra observed by doppler sounding systems. *Radio Sci.,* **20,** 1323-1330.

VanZandt, T.E., Smith, S.A., and Fritts, T.E., 1985. Gravity wave spectra observed by doppler radar: comparison of a model with mesospheric observations. *Handbook for MAP,* **18,** 212-215, SCOSTEP Secretariat, Univ. IL, Urbana.

Vergeiner, I., and Lilly, D., 1970. The dynamic structure of lee wave flow as observed from balloon and airplane observation. *Mon. Wea. Rev.,* **98,** 220-232.

Vincent, R.A., 1985. Radar observations of mesoscale gravity waves and turbulence at Adelaide. *Handbook for MAP,* **18,** 196-200, SCOSTEP Secretariat, Univ. IL, Urbana.

Wooldridge, G., and Reiter, E.R., 1970. Large-scale atmospheric circulation characteristics as evident from GHOST balloon data. *J. Atmos. Sci.,* **27,** 183-194.

Yamanaka, M.D., and Tanaka, H., 1984. Meso- and microscale structures of stratospheric winds: a quick look at balloon observations. *J. Meteor. Soc. Japan,* **62,** 177-182.